Three-Dimensional Phenomena in Microbubble Acoustic Streaming

Alvaro Marin,[1] Massimiliano Rossi,[1] Bhargav Rallabandi,[2] Cheng Wang,[2,3] Sascha Hilgenfeldt,[2] and Christian J. Kähler[1]

[1]*Institut für Strömungsmechanik und Aerodynamik, Bundeswehr University Munich,*
85577 Neubiberg, Germany
[2]*Department of Mechanical Science and Engineering, University of Illinois at Urbana-Champaign,*
1206 West Green Street, Urbana, Illinois 61801, USA
[3]*Department of Mechanical and Aerospace Engineering, Missouri University of Science and Technology,*
194 Toomey Hall, Rolla, Missouri 65409, USA

Ultrasound-driven oscillating microbubbles are used as active actuators in microfluidic devices to perform manifold tasks such as mixing, sorting, and manipulation of microparticles. A common configuration consists of side bubbles created by trapping air pockets in blind channels perpendicular to the main channel direction. This configuration consists of acoustically excited bubbles with a semicylindrical shape that generate significant streaming flow. Because of the geometry of the channels, such flows are generally considered as quasi-two-dimensional. Similar assumptions are often made in many other microfluidic systems based on flat microchannels. However, in this Letter we show that microparticle trajectories actually present a much richer behavior, with particularly strong out-of-plane dynamics in regions close to the microbubble interface. Using astigmatism particle-tracking velocimetry, we reveal that the apparent planar streamlines are actually projections of a stream surface with a pseudotoroidal shape. We, therefore, show that acoustic streaming cannot generally be assumed as a two-dimensional phenomenon in confined systems. The results have crucial consequences for most of the applications involving acoustic streaming such as particle trapping, sorting, and mixing.

Introduction.—Among the vast amount of microfluidics systems that have been emerging since the late 1990s, those involving the use of acoustic fields to enhance flow control (i.e., acoustofluidics) have experienced great development in recent years due to their practical simplicity, versatility, and potentiality for applications as particle separation [1–3], particle trapping [4], acoustic manipulation of droplets using surface acoustic waves [5,6], or acoustic centrifugation [7]. Direct piezoelectric actuation of microchannel walls generates acoustic waves whose interaction with suspended particles through streaming flows or radiation forces is used to concentrate, trap, or separate them through either acoustic streaming (interaction with the fluid) or radiation forces (interaction with the particles) [8–10]. However, other types of applications may require higher shear stresses or just a different range of frequencies than those achievable by standing acoustic waves. Instead of actuating directly on the solid boundary of the channel, an alternative is to actuate on the surface of a sessile microbubble that is deliberately created in the system. The kHz-frequency oscillations of the bubble surface then generate a steady streaming flow of adjustable intensity. Such a technique is particularly effective in soft-wall microfluidic systems such as PDMS (polydimethylsiloxane) devices, where waves in the substrate are strongly damped. Ultrasound-driven microbubble streaming flows have been studied for applications to promote fluid transport [11], manipulation and poration

of vesicles [12], and, more recently, for applications such as particle separation and trapping [13,14].

One of the simplest and most natural configurations to insert stable sessile microbubbles in PDMS microchannels is to create blind side channels. When the channel is filled with water, gas is retained in the pocket which then adopts a semicylindrical shape (Fig. 1). Because of the lithography-based microfabrication, a 2D planar geometry is imposed, and a reasonable assumption is that the two-dimensional shape of the channel and its semicylindrical bubble shape damps the third component of the flow field, leaving a 2D flow profile. The assumption has been proven valid enough to study general aspects of the phenomenon as the
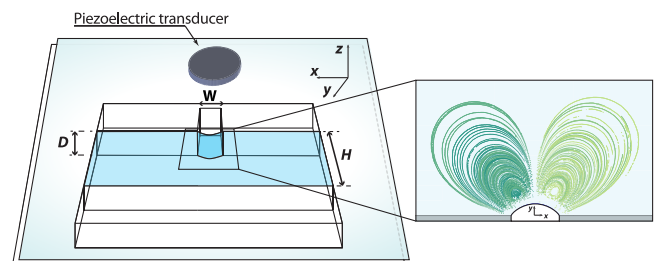

FIG. 1. Typical experimental setup. Left: The PDMS channel and the piezoelectric actuator are bonded to a glass slide. Right: Top view of the semicylindrical bubble in the microchannel and visualization of the acoustic streaming flow through different experimental particle trajectories.
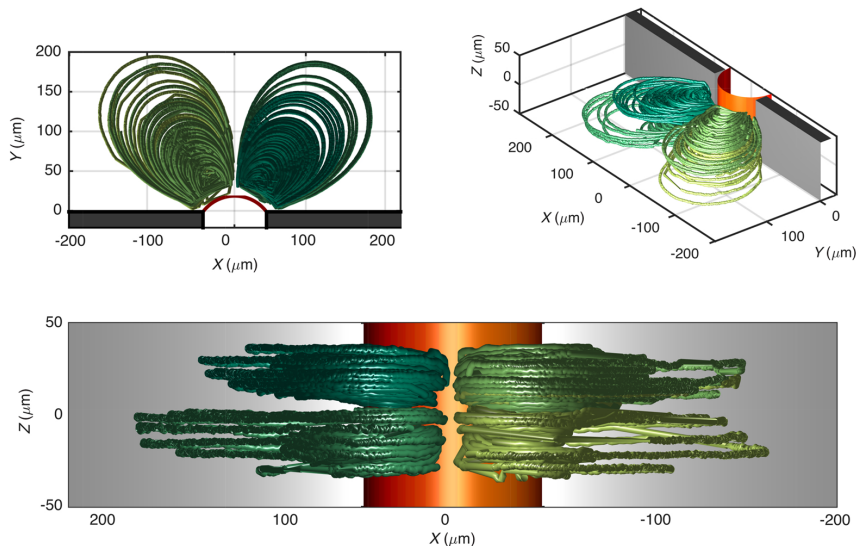
FIG. 2. Trajectories of four different particles. Top left: Projection of particles' trajectories in the XY plane. Top right: Orthographic projection of the particle trajectories. Bottom: Projection of particles' trajectories in the XZ plane. The symmetry planes (midplane or transverse plane at $z = 0$ and sagittal plane at $x = 0$) are clearly visible in the figure. A third plane of symmetry (coronal plane at $y = 0$) should appear for perfectly cylindrical bubbles. Instead, our system allocates the channel wall at that position, altering the global symmetry of the system.

typical frequency resonances [15] or the two-dimensional streaming flow by using asymptotic models [16].

In this Letter, we demonstrate through experimental measurements that particles do experience off-plane dynamics in the vicinity of the microbubble, which reveals an unexpected degree of complexity in confined fluidic systems driven by acoustic streaming. Here we will describe the dynamics of the complex flow, point out the consequences for applications, as well as determine in which circumstances one can ignore the three-dimensional features of the flow. In order to inquire on the nature of the flow, a three-dimensional solution of the Stokes equation showing the same trend can be constructed, which compares well with the experimental results. A more detailed description of the theoretical model will be shown in a companion paper [17].

Experimental setup.—The microfluidic device is made of PDMS by soft lithography: the PDMS components are blended at a 10:1 ratio, degassed, and poured into an SU-8 mold to cross-link for 24 h. The cured PDMS is then bonded to a glass slide via oxygen-plasma treatment. Typical microchannels (see Fig. 1) have a height $D = 100$ μm, and a width $H = 1000$ μm, while the blind channel holding the semicylindrical microbubble has a typical width $W = 80$ μm. The microbubble is driven by ultrasound actuation through a piezoelectric transducer (10 mm diameter, Physik Instrumente, Germany) glued to the glass slide, next to the PDMS channel (Fig. 1). An amplified sinusoidal signal is sent to the transducer through a function generator GW-Instek AFG-2125. All experiments here are made at a typical frequency of approximately 20 kHz, appropriate for strong excitation of microbubbles of the present size [15]. In order to acquire more data at sufficient resolution, the flow can be slowed down by choosing a lower voltage at the piezoelectric transducer.

3D particle tracking.—The particle trajectories and velocities are measured using astigmatism particle-tracking velocimetry (APTV) [18,19]. APTV is a single-camera particle-tracking method in which an astigmatic aberration is introduced in the optical system by means of a cylindrical lens placed in front of the camera sensor. Consequently, an image of a spherical particle obtained in such a system shows a characteristic elliptical shape unequivocally related to its depth position z. The images of the particles in the microfluidic chip are taken using an inverted microscope Zeiss Axiovert in combination with a high-speed CCD camera PCO.dimax at recording speeds in the range from 500 to 1000 frames/sec. The optical arrangement consists of a Zeiss Plan-Neofluar $20\times/0.4$ microscope objective lens and a cylindrical lens with focal length $f_{\rm cyl} = 150$ mm placed in front of the CCD sensor of the camera. Monodisperse fluorescent spherical polystyrene particles with nominal diameters of 2 μm (Microparticles GmbH) are used for the experiments ($\rho_{\rm ps} = 1050$ kg m^{-3}). Illumination is provided by a continuous-diode-pumped laser with 2-W power at 532-nm wavelength. This configuration provides a measurement volume of $600 \times 600 \times 120$ μm^3 with an estimated uncertainty in the particle position of ± 1 μm in the z direction and less than ± 0.1 μm in the x and y directions. The particle trajectories detected for this frequency vary in length and in time scale and add up to more than 50 different trajectories. More details about the experimental configuration and uncertainty estimation of the APTV system can be found in Ref. [19].

Results.—Figure 2 shows measured trajectories corresponding to four selected particles. Each trajectory occupies different volumes separated by two planes of symmetry: the midplane $z = 0$ and the bubble's sagittal plane $x = 0$. A third symmetry plane would be expected if the bubble were perfectly cylindrical. Most of the observed particles are confined in between the symmetry planes, but particles crossing the symmetry planes are also eventually observed. Some selected trajectories are animated in the Supplemental Material [20].
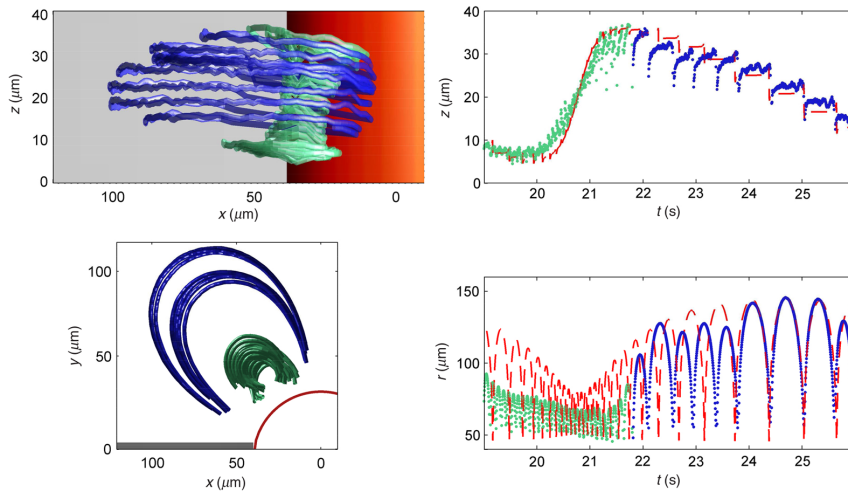
FIG. 3. Detail of a typical particle trajectory. The green and blue paths depict, respectively, the inner and outer particle loops, in which the particle travels, respectively, away from and towards the midplane $z = 0$. Left: Projection of the particle in the ZX plane (top) and in the XY plane (bottom). Top right: Particle vertical distance from the system's midplane $z = 0$; notice the jumps that the particle performs when closely approaching the bubble's surface. The red discontinuous line shows the results from simulations. Bottom right: Radial distance $r = \sqrt{x^2 + y^2}$ from the bubble's symmetry axis in time.

Figure 3 illustrates a portion of a trajectory: particles follow an almost flat trajectory at large r but experience discrete "jumps" into a different plane every time the particle's orbit reaches its perigee, i.e., when the particle comes to its closest distance to the bubble's surface ($r_{\min}$). Particle trajectories typically follow a periodic pattern similar to the one depicted in Fig. 3: the particle starts close to the midplane $z = 0$ with a series of fast loops characterized by short periods, short apogees (farthest position from the bubble's surface $r_{\max}$), and large perigees (trajectory in green in Fig. 3). When passing through the perigee, the particle suffers small jumps away from the midplane. As the particle approaches the channel ceiling or floor, the orbit reduces the perigee, enlarges its apogee, and, consequently, its period becomes longer (blue trajectory in Fig. 3). Now, the particle jumps towards the midplane every time it hits its perigee. As the particle approaches the midplane again, the orbit decreases its apogee, reduces its perigee, and will repeat the same pattern again. This particular trajectory is animated in a video in the Supplemental Material [20]. Since particles suffer strong velocity gradients, when choosing the experimental settings, one faces a dilemma: either to resolve the short-time-scale particle dynamics or the long-time-scale dynamics. Since our objective is to get a general view of the particle orbit, we choose the latter option. Therefore, note from the bottom plots in Fig. 3 that the selected experimental settings do not allow us to resolve experimentally the portion of the particle trajectory closest to the bubble, and, therefore, the streamlines are not closed.

Another remarkable symmetry becomes visible when observing the velocity field in detail in Fig. 4: as particles approach the bubble at low angles θ, they are advected into the bubble's horizontal plane $z = 0$ at $\theta < 60°$ and immediately after at $\theta > 60°$ away from it. Once the particle leaves the bubble behind, there is a net displacement in its z position whose direction and value depend strongly on the relative position to the bubble. Interestingly enough, the critical angle $\theta \approx 60°$ at which the value of V_z changes sign corresponds also to the angle at which V_r changes sign and to the position at which V_θ reaches its maximum value (Fig. 4). It is interesting to note that in the horizontal plane $z = 0$, V_θ and V_r reach their maximum values, while V_z reaches a minimum. In the data shown, the maximum Reynolds number that a 2-μm particle experiences is $\mathrm{Re}_p \sim 10^{-2}$, and, therefore, inertial effects do not play any role. However, even though the flow is clearly viscous, stresses can be significant. For example, the maximum shear rates experienced at the top or bottom walls can be as high as 500 s^{-1}, while in the bulk they reach 1000 s^{-1}. Note that mechanisms as shear-induced migration cannot be invoked to explain the particle dynamics due to the low-particle seeding employed in our experiments. It is normally assumed that the streamlines are two dimensional and mostly closed [21]. However, when observing the planar projection, one can observe particle paths crossing streamlines. It is normally concluded that the particle is perturbed by the bubble surface oscillations, forcing the particle to change streamlines [14]. Although such a mechanism is valid and probably occurs as well, the present results show that apparent streamline crossings are also caused by the particle following a complex 3D stream surface that has a toroidal shape (Fig. 3). That explains why apparent streamline crossing occurs even for very small tracer particles. Interestingly enough, particles are very rarely seen making a full and closed 3D trajectory. The most likely reason is that the time required to go through the full three-dimensional orbit (a full period) is much longer than our observation time. Still, streamline crossing cannot be totally neglected since the chances of a perturbation to occur while the particle travels are higher for longer periods.

Discussion.—Secondary flows unavoidably appear in three-dimensional systems even at low Reynolds numbers when a streamwise component of vorticity is developed in the presence of a boundary layer. A classical example of
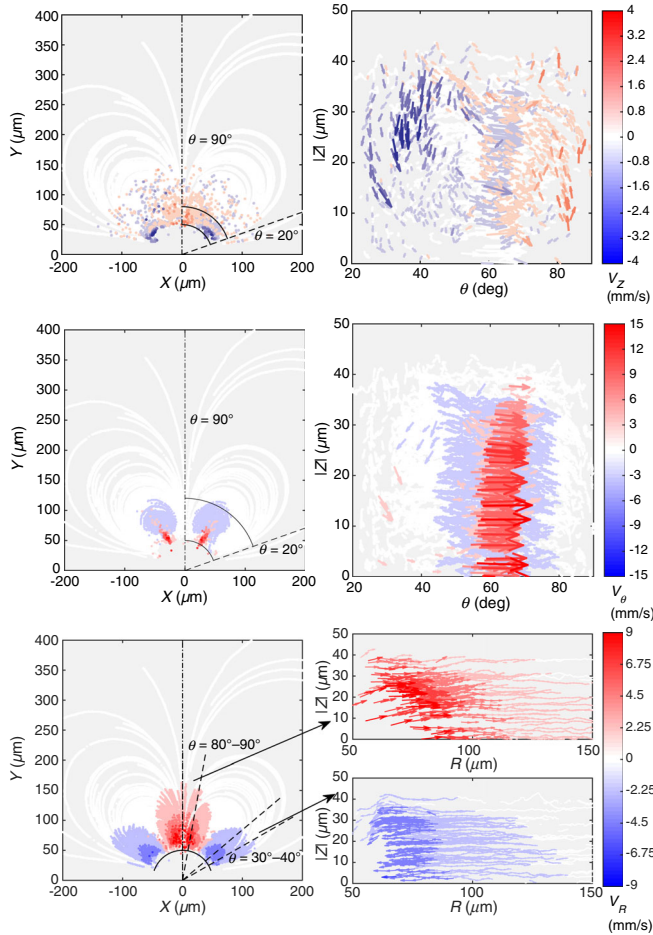
FIG. 4. Particle velocity distributions. Top: Off-plane velocity component V_z; note that they only become significant in the vicinity of the bubble's surface. The arcs drawn in the top left figure represent the section plotted in the top right plot. Middle: Azimuthal velocity component V_θ. Bottom: Radial velocity V_r with maximum values at the sagittal plane and at approximately $\theta = 30°$ (bottom right plots).

secondary flow is the so-called tea-leaf effect [22], which explains why particles concentrate in the bottom center of a stirred tea cup, but they are also present when a pipe flow enters a bend or over an immersed rotating disk. In our particular case, in addition to this common phenomenon, we must add the effect of the oscillations along the axis of the cylindrical bubble, which cannot be neglected. These effects can be taken into account by a modification of the two-dimensional bubble streaming solution, which is governed by a stream function $\psi_{2D}(r, \theta)$ [16,17]. Because of the small Reynolds number associated with the streaming, it is appropriate to seek a linear superposition involving ψ_{2D} and axial solutions of the Stokes equations satisfying no penetration conditions at the bubble and the walls of the microchannel, as well as the appropriate symmetries about $x = 0$ and $z = 0$ observed in the experiment. The lowest-order axial solution (weakest radial decay) is axisymmetric and is governed by a Stokes stream function ψ_{ax} of the form

$$
\psi_{ax}(r, z)
$$
$$
= u_s a \frac{r}{a} \left(\frac{K_2(2\pi r/D)}{K_2(2\pi a/D)} - \frac{K_0(2\pi r/D)}{K_0(2\pi a/D)} \right) \sin(2\pi z/D). \tag{1}
$$

Here, u_s is the characteristic scale of the streaming near the bubble surface (quadratic in driving voltage), $a = W/2$ is the bubble radius, and K_ν represents a modified Bessel function of the second kind. The velocity field due to the superposition of 2D and axisymmetric modes is formally given by

$$
\mathbf{u}(r, \theta, z) = \nabla \times \{\psi_{2D}(r, \theta)\hat{\mathbf{z}} + c_{ax}\psi_{ax}(r, z)\hat{\theta}\}, \tag{2}
$$

where $0 < c_{ax} \ll 1$ sets the relative strength of the axial flow and is used as a fit parameter between the theory and experiment. Figure 3 shows that fluid trajectories under the linear superposition (2) qualitatively agree with experimentally measured particle trajectories over short (approximately milliseconds) and long (approximately seconds) time scales.

The results here may also have crucial consequences in stirring or mixing in microfluidic viscous flows. From Aref [23] and Ottino [24] we learn that in order to enhance mixing in viscous flows, one must generate striations or tendrils thin enough to increase the value of the gradients and to allow diffusion to transfer mass in reasonable time scales. In this sense, 3D flows can achieve better mixing rates even in a passive way since they stretch and fold the liquid more efficiently, as is shown by the Herringbone mixer [25] or the 3D serpentine [26]. The three-dimensional character of streaming flow from a semi-cylindrical bubble contributes to the good mixing that can be already achieved in the liquid surrounding one single bubble. Mixing can be further enhanced by simply adjusting the bubble's aspect ratio to enhance 3D effects, in addition to modulating its actuating frequency or adding more bubbles in different 3D positions [15].

Conclusions and Outlook.—In this Letter, we show that the previously assumed 2D character of acoustic streaming by semicylindrical bubbles does not hold when particles approach the bubble's vicinity. Instead, 3D flow effects are present, which have crucial consequences on the particle trajectories and, therefore, on the fluid flow surrounding the bubble. The mechanisms driving such a flow must necessarily be connected with the presence of axial bubble oscillations and their necessary fulfillment of the boundary conditions.

[1] F. Petersson, A. Nilsson, H. Jönsson, and T. Laurell, Carrier medium exchange through ultrasonic particle switching in microfluidic channels, Anal. Chem. 77, 1216 (2005).

[2] T. Laurell, F. Petersson, and A. Nilsson, Chip integrated strategies for acoustic separation and manipulation of cells and particles, Chem. Soc. Rev. 36, 492 (2007).

[3] P. Augustsson, R. Barnkob, S. T. Wereley, H. Bruus, and T. Laurell, Automated and temperature-controlled micro-PIV measurements enabling long-term-stable microchannel acoustophoresis characterization, Lab Chip 11, 4152 (2011).

[4] B. Hammarström, M. Evander, H. Barbeau, M. Bruzelius, J. Larsson, T. Laurell, and J. Nilsson, Non-contact acoustic cell trapping in disposable glass capillaries, Lab Chip 10, 2251 (2010).

[5] J. Friend and L. Yeo, Microscale acoustofluidics: Microfluidics driven via acoustics and ultrasonics, Rev. Mod. Phys. 83, 647 (2011).

[6] T. Franke, A. R. Abate, D. A. Weitz, and A. Wixforth, Surface acoustic wave (SAW) directed droplet flow in microfluidics for PDMS devices, Lab Chip 9, 2625 (2009).

[7] R. V. Raghavan, J. R. Friend, and L. Y. Yeo, Particle concentration via acoustically driven microcentrifugation: MicroPIV flow visualization and numerical modelling studies, Microfluid. Nanofluid. 8, 73 (2010).

[8] H. Bruus, Acoustofluidics 2: Perturbation theory and ultrasound resonance modes, Lab Chip 12, 20 (2012).

[9] H. Bruus, Acoustofluidics 7: The acoustic radiation force on small particles, Lab Chip 12, 1014 (2012).

[10] P. B. Muller, M. Rossi, A. Marin, R. Barnkob, P. Augustsson, T. Laurell, C. J. Kähler, and H. Bruus, Ultrasound-induced acoustophoretic motion of microparticles in three dimensions, Phys. Rev. E 88, 023006 (2013).

[11] P. Marmottant, J. P. Raven, H. J. G. E. Gardeniers, J. G. Bomer, and S. Hilgenfeldt, Microfluidics with ultrasound-driven bubbles, J. Fluid Mech. 568, 109 (2006).

[12] P. Marmottant, T. Biben, and S. Hilgenfeldt, Deformation and rupture of lipid vesicles in the strong shear flow generated by ultrasound-driven microbubbles, Proc. R. Soc. A 464, 1781 (2008).

[13] C. Wang, S. V. Jalikop, and S. Hilgenfeldt, Size-sensitive sorting of microparticles through control of flow geometry, Appl. Phys. Lett. 99, 034101 (2011).

[14] C. Wang, S. V. Jalikop, and S. Hilgenfeldt, Efficient manipulation of microparticles in bubble streaming flows, Biomicrofluidics 6, 012801 (2012).

[15] C. Wang, B. Rallabandi, and S. Hilgenfeldt, Frequency dependence and frequency control of microbubble streaming flows, Phys. Fluids 25, 022002 (2013).

[16] B. Rallabandi, C. Wang, and S. Hilgenfeldt, Two-dimensional streaming flows driven by sessile semicylindrical microbubbles, J. Fluid Mech. 739, 57 (2014).

[17] B. Rallabandi, A. Marin, M. Rossi, C. J. Kähler, and S. Hilgenfeldt, Three-dimensional streaming flow in confined geometries (to be published).

[18] C. Cierpka, M. Rossi, R Segura, and C. J. Kähler, On the calibration of astigmatism particle tracking velocimetry for microflows, Meas. Sci. Technol. 22, 015401 (2011).

[19] M. Rossi and C. J. Kähler, Optimization of astigmatic particle tracking velocimeters, Exp. Fluids 55, 1809 (2014).

[20] See the Supplemental Material at http://link.aps.org/supplemental/10.1103/PhysRevApplied.3.041001 for a video showing different particle three-dimensional trajectories and for an animated version of Fig. 3.

[21] P. Marmottant, M. Versluis, N. de Jong, and S. Hilgenfeldt, High-speed imaging of an ultrasound-driven bubble in contact with a wall: "Narcissus" effect and resolved acoustic streaming, Exp. Fluids 41, 147 (2006).

[22] A. Einstein, Die Ursache der Mäanderbildung der Flussläufe und des sogenannten Baerschen Gesetzes, Naturwissenschaften 14, 223 (1926).

[23] H. Aref, Stirring by chaotic advection, J. Fluid Mech. 143, 1 (1984).

[24] J. M. Ottino, The Kinematics of Mixing: Stretching, Chaos, and Transport (Cambridge University Press, Cambridge, England, 1989), Vol. 3.

[25] A. D. Stroock, S. K. W. Dertinger, A. Ajdari, Igor Mezić, H. A. Stone, and G. M. Whitesides, Chaotic mixer for microchannels, Science 295, 647 (2002).

[26] R. H. Liu, M. A. Stremler, K. V. Sharp, M. G. Olsen, J. G. Santiago, R. J. Adrian, H. Aref, and D. J. Beebe, Passive mixing in a three-dimensional serpentine microchannel, J. Microelectromech. Syst. 9, 190 (2000).